Available online at sjuoz.uoz.edu.krd

Science Journal of University of Zakho

Vol. 11, No. 2, pp. 286– 297, April-June, 2023

journals.uoz.edu.krd

p-ISSN: 2663-628X
e-ISSN: 2663-6298

THE EFFECT OF CALCINATION TEMPERATURES ON THE PROPERTIES OF ZNO NANOPARTICLES SYNTHESIZED BY USING LEAVES EXTRACTS OF PINUS BRUTIA TREE

Sherwan M. Mahdi Ismail [1*], Sabah M. Ahmed [1]

1 Department of Physics, College of Science, University of Duhok, Kurdistan Region, Iraq

Received: 15 Dec., 2022 / Accepted: 8 Jan., 2023 / Published: 7 June, 2023 *https://doi.org/10.25271/sjuoz.2023.11.2.1087*

ABSTRACT:

Pinus Brutia (PB) tree leaf extracts were used to produce zinc oxide (ZnO) nanoparticles. The study of the PB tree extracts at several calcination temperatures from (200 to 500) ºC on the formation of ZnO NPs' characteristics has been investigated using various characterization techniques. The chosen plant PB had its findings at both examinations of FTIR and UV-Visible spectroscopies shown and offered to be a superior option for the GS ZnO NPs at various pH levels. PB tree leaf extracts' UV-visible spectra revealed one distinguishable absorption peak at 275.3 nm. The study of the FESEM results showed that the Green Synthesized (GS) ZnO NPs' orientation, shape, and dimensions are significantly impacted by the calcination temperatures. The ZnO NPs are also shown by the XRD data to have hexagonal wurtzite crystal structures that have particle sizes at (002) peak falling within the range between (10 to 24) nm. The UV-Visible study of the ZnO NPs showed a strong peak absorbance for ZnO NPs that were calcined at various temperatures, with high UV absorption below 400 nm. The obtained energy band gap (E_g) is located in the region between (2.65 and 2.747) eV, narrowing as the calcination temperature rises. The ZnO NPs that were calcined at a temperature of 500 ºC also had superior quality and outperformed those produced at other calcination temperatures, according to all of the analyzed results and properties of the ZnO NPs.

Keywords: Calcination Temperature, ZnO NPs, Pinus Brutia, Green Method, Tree Extract

1. INTRODUCTION

One of the most rapidly developing and ever-evolving fields is nanotechnology, regarded as the industrial revolution of this time. With the potential to form and underpin an advancement in a wide range of biotechnology and technology (Azeez et. al., 2020). Many research and commercial fields, including electronics, information technology, biology, agriculture, chemistry, and physics, have used nanotechnology (Abdelbaky et. al., 2022). Due to the advanced chemical and biological properties of nanoparticles, they have many applications in science. These advanced properties of nanoparticles can't be found in the bulk material of the same chemicals (Khan et. al., 2019).

The unique property of nanoparticles (NPs) is that they have a high surface-to-volume ratio. This makes them good candidates for performance-oriented applications like cosmetics, creating gas sensors, energy storage, electronics devices, food packaging, and environmental remediation, which promotes their incorporation into a wide range of technology (Nilavukkarasi et. al., 2020; Zheng, et. al., 2020). It is believed that metal oxide nanoparticles are more advantageous than other nanoparticles due to their unique physical, chemical, and biological properties (Waseem et. al., 2020). ZnO nanoparticles, known for their remarkable piezoelectric, optoelectronics, pyroelectric, semiconducting, catalysis, and antimicrobial properties, are among them. They have been recognized as a material with great potential in all fields, such as physics, biology, engineering, chemistry, and so on (Bettini et. al., 2015; Hong et. al., 2011).

Numerous negative side effects and toxicities are brought on by the reduction and capping of nanoparticles with toxic chemicals. Consequently, the use of plant extracts in the synthesis of metal oxide nanoparticles has grown in significance (Meron et. al., 2020). Compared to conventional chemicals, this method is more environmentally friendly and has a quicker reaction time. Plant extracts have a variety of bioactive molecules that help stabilize and reduce nanoparticles (Seyyed et. al., 2020). According to past research, researchers managed to form Zinc Oxide NPs through plant extracts; a large number of plants that are used to synthesize ZnO NPs can be found in literature, for example, Trifolium pratense, Aloe vera, Vitex trifolia, Matricaria chamomilla, Camellia sinensis, Azadirachta indica, Artocarpus gomezianus, Olea europaea, and Duranta erecta (Meron et. al., 2020).

A green chemical and environmentally benign approach for the synthesis of zinc oxide (ZnO) nanostructure has been explored using aqueous solution of Gum Arabic (GA) (Taha et. al., 2019). Agarwal et. al. (2019) focus on the fabrication of nano-sized ZnO particles by using zinc oxide as a precursor molecule and leaf extract of Cinnamomum Tamala as a reducing and capping agent. The structural analysis confirmed that copper ions substitute Zn ions without altering their wurtzite structure and a crystallite size of 10–16 nm with high degree of crystallization (Vanaja et. al., 2019). Kanimozhi et. al. (2019) have prepared zinc oxide by high pressure homogenization process and the resultant zinc oxide was evaluated as fibers in CS/PVA/MC3 films. Gahlawat et. al. (2019) reviewed the progress made in recent years on nanoparticle biosynthesis by microbes. Zhou et. al. (2020) present a highly selective transformation of methane to methanol using gold modified zinc oxide as a photocatalyst under full light spectrum irradiation at atmospheric temperature. Chauhan et. al. (2020) explore removal of carcinogenic cationic and anionic dyes from aqueous medium using green fabricated zinc oxide nanoparticles (ZnO-NPs). Plants contain biomolecules that can act as capping, oxidizing and reducing agents that increase the rate of reaction and stabilizes the NPs. Rahman et. al. (2021) emphasize and compiles different types of plants and parts of plant used for the synthesis of ZnO and its potential applications at one place. Other influential work includes (Patil et. al., 2020 and Sekar et. al., 2021).

The subject of (Faye et. al., 2021) was to synthesise ZnO and nickel doped ZnO nanoparticles using Euphorbia abyssinica bark extract for antimicrobial activity studies via agar disk diffusion method against some selected microbes. Diab et. al. (2022)

* Corresponding author

evaluate the effects of green-synthesized zinc oxide nanoparticles (ZnO-NPs) using Ulva fasciata extract as an anti-fungal agent against Candida albicans (C. albicans) in vitro and in vivo in O. niloticus. Irfan et. al. (2022) develop zinc oxide nanoparticles (ZnO-NPs) based surgical sutures for the accelerated wound healing process. The NPs synthesized by the method are also free from toxicity properties. Chandrasekaran et. al. (2022) describe one such green synthesis method for zinc oxide nanoparticles (ZnO NPs) using the aqueous flower extract of Senna auriculata. Biogenic ZnO NPs were synthesized using seed extract by a simple, cost-effective, and green chemistry approach (Sakthivel et. al., 2022).

This study was aimed at the environmentally friendly fabrication of ZnO-NPs from plant extract (Awan et. al., 2022). Other influential work includes (Ari et. al., 2021; Hasan et. al., 2022; Nitnavare et. al., 2022 and Mutukwa et. al., 2022).

This research focuses on the production of ZnO nanoparticles through the green method from Pinus Brutia (PB) tree leaf extracts. The effect of different calcination temperatures in the range of (200 to 500) ^{o}C on the quality characteristics of GS ZnO NPs has been studied. The importance of this research is highlighted by a thorough examination of the various factors that influence the shape, size, particle size distribution, optical properties, crystal structure, and energy band gap of ZnO NPs. The role of green plant biomolecules in the bioreduction of metal salts during nanoparticle extraction has been demonstrated.

2. EXPERIMENTAL METHOD

The zinc salt (Zinc nitrate hexahydrate) [Zn $(NO_3)_2$. $6H_2O$] with molecular weight (297.48 g/mol) and purity greater than (99%) as well as sodium hydroxide powder [(NaOH) molecular weight (40 g/mol)] were purchased from Sigma-Aldrich and used for this study with no further treatment.

The 60 grams of fresh green PB tree leaves were collected, washed thoroughly with distilled water to remove any dust or pollution, cut into small pieces, and then placed in 600 ml of distilled water. The mixture was heated at 75 ^{o}C for 50 minutes, after which the PB leaf extracts were filtered many times using filter paper with pore sizes of 8 µm and centrifuged extensively (Karam et al., 2022). The characterization using a UV-V spectrometer and FTIR were checked, and the extracts were stored in a cold place for future use.

To prepare the GS ZnO NPs at different calcination temperatures, 60 ml of PB tree extracts from the leaf were added dropwise to (0.1 M) in 60 ml of zinc nitrate hexahydrate [Zn (NO3)2. 6H2O] dropwise under magnetic stirring at 75 ^{o}C degrees for 30 minutes. Later, the pH of the prepared GS mixture was adjusted to 8 by adding drops of (NaOH) sodium hydroxide while the magnetic stirrer was turned on. A pH meter was used to monitor the pH of the solution continuously. The color and transparency of the mixture began to change as the pH was adjusted, indicating that a reaction between the metal salt and the plant extracts occurred, and ZnO NPs were formed. For 8 hours, the setup was kept on magnetic stirring at 75 ^{o}C until all of the water evaporated (Amad et. al. 2022). After 8 hours on the heater stirrer, the leftovers from the mixture were calcined and purified in the annealing furnace for 2 hours at several calcination' temperatures. The final product of GS ZnO NPs was then stored in a tube for characterization, as shown in Figure 1. For different calcination temperatures of the GS mixture, such as (200, 300, 400, and 500) ^{o}C and the fabricated samples were labeled (a), (b), (c), and (d), respectively.

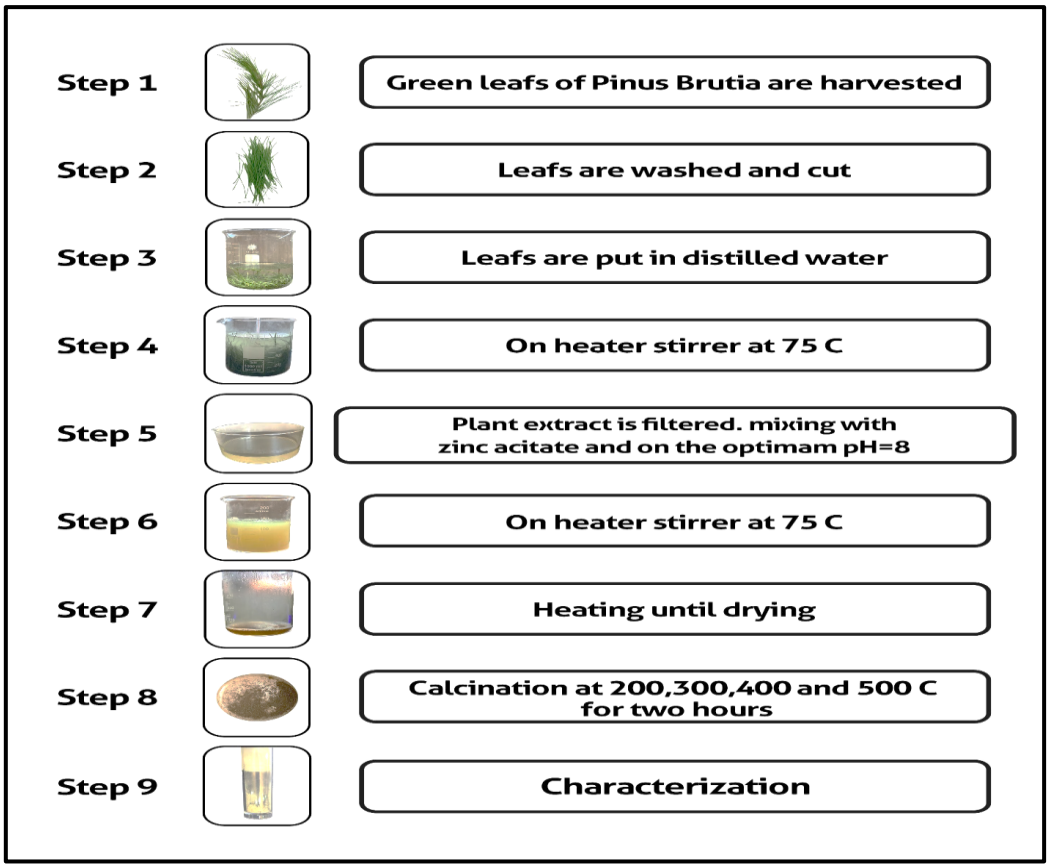

Figure 1. Schematic Diagram representation of the ZnO NPs using Green Synthesized at different Calcinations Temperatures using Leaf extracts of the PB tree.

PB tree leaf extracts and the resulting Zinc Oxide nanoparticles are examined using a UV-Visible double beam spectrophotometer by Agilent Technologies carrier series to determine their optical characteristics (Cary 100 UV-Vis). The wavelengths of absorption of ZnO NPs and leaf extracts were measured between 200 and 800 nm. A surface study including

shape, chemical composition, size, and orientation of ZnO NPs, studying the size and crystal formation, stress and strain, and quality of the produced Zinc Oxide nanoparticles at different calcination temperatures were all carried out using PB leaf extracts and the various functional groups that appeared in them (Nicolet IS10, Thermo Scientific, Waltham, MA, USA).

The testing range for Fourier Transform Infrared Spectroscopy (FTIR) was set to begin at 400 to 4000 cm-1, followed by using the Supra 55VP from Carl Zeiss AG. We performed (EDX) energy-dispersive X-ray spectroscopy and (FE-SEM) field emission scanning electron microscopy with CuK radiation at 1.54050 angstroms and scanning angles between 20 and 80 degrees.

3. RESULTS AND DISCUSSION

The Fourier Transform functional groups (FTIR) associated with reductive biomolecules have been investigated using infrared of the tree extract spectra and the functional groups that support the reduction of ZnO (Aswathy et. a., 2021; Barzinjy et. al., 2020). Figure 2 depicts the FTIR spectrum of the PB tree leaf extracts. As can be seen, this spectrum exhibits many peaks between (400- 4000) cm^{-1}. In essence, the FTIR spectrum may be separated into two regions: first, from (0-1500) cm^{-1} is the region that can be called the fingerprint; in this region, it is possible to see that plant extract that is utilized to create ZnO nanoparticles. Second, the functional group region spans the range of (1800-4000) cm^{-1}. FTIR spectra typically provide information about the composition of internal components that connect all stages of matter (Norouzi et. al., 2019; Srivastava, et. al. 2013 and Zandi et. al., 2011). Peak absorption at 815 cm^{-1} is mostly caused by C-H bond 1,4-disubstitution (para). The phosphate ion of common inorganic ions is the peak that was observed at 1072 cm^{-1}. The measured absorption peak for the aryl-O stretch of ether and oxy molecule, which includes aromatic ethers, is at 1253 cm^{-1}. At 1340 cm^{-1}, CN stretch, the aromatic primary amine is at its highest absorption. Additionally, the peak of primary amine, or 1608 cm^{-1} NH bend, is seen. The 2931 cm^{-1} peak under investigation is a Methylene C-H asym./sym. stretch (>CH2). The aliphatic secondary amine and >N-H stretch of secondary amino, respectively, peak at 3334 cm^{-1} and 3363 cm^{-1}. Additionally, aliphatic primary amine and NH stretch peaks at 3385 cm^{-1}. Meanwhile, the obtained peak at 3421 cm^{-1} is an NH stretch and an aromatic primary amine (Kim et. al., 2001).

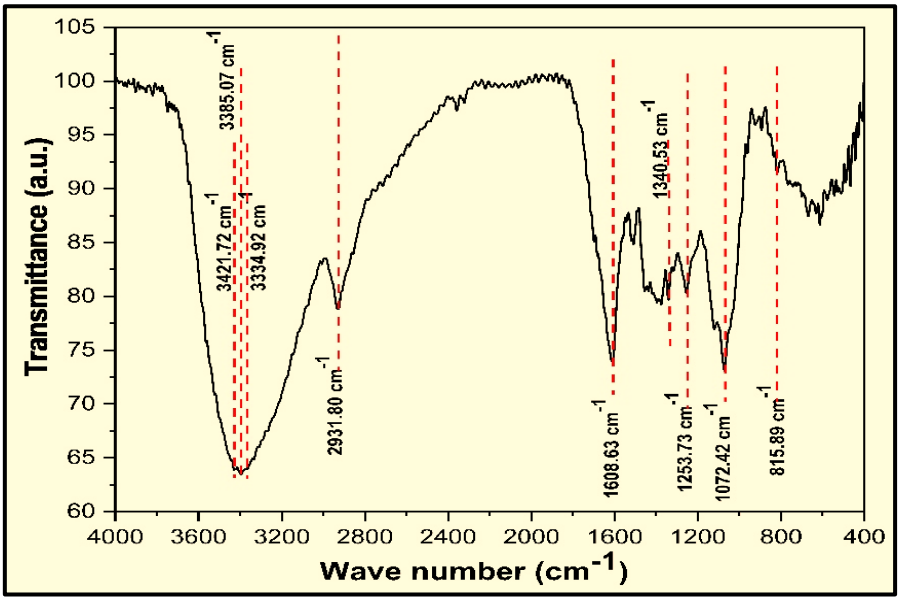

Figure 2. FTIR Spectrum Analysis of the PB Tree Leaf Extracts

The leaf extracts' UV-visible spectrum of the PB tree is shown in Figure 3. One maximum peak was visible at a wavelength of (275.3) nm. This peak can be explained by the phytochemicals found in the leaf extracts of the PB tree, which is plausible given that OH groups serve as numerous stabilizing agents. NPs can be created by bio-reducing (Singh et. al., 2016). Since these phytochemicals are antioxidants and free of hazardous substances, they continue to be very effective at reducing metal ions and their stability at the nanoscale. Phytochemicals can produce nanoparticles of varied shapes and sizes simultaneously (Hocine et. al., 2016). Electromagnetic waves carry out the creation of NPs, and the spectra of the (UV-Vis.) indicated the absorption peak (SPR) surface plasmon resonance and retains electron (e) oscillations in the conduction-band reactive metal ion reduction (Pai 2019).

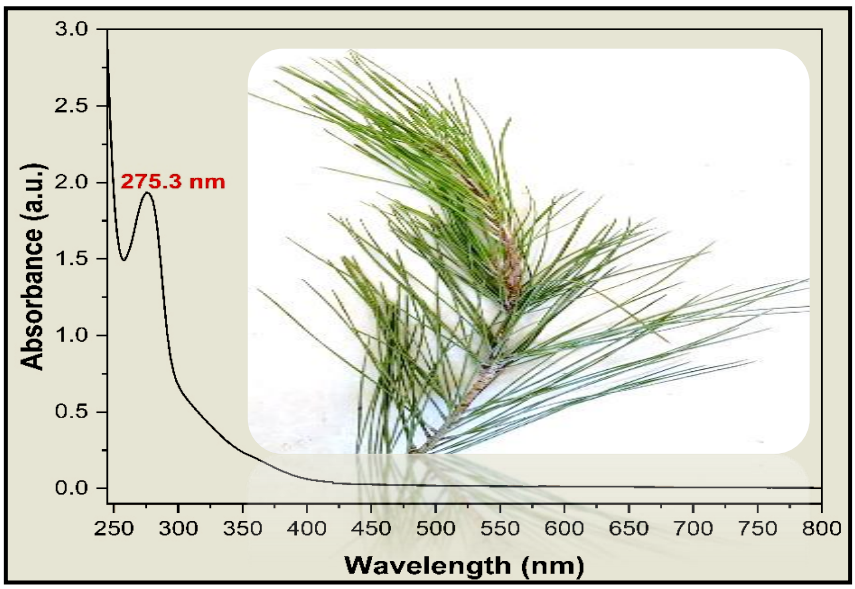

Figure 3. UV-Vis. Spectrum Analysis of the Pinus Brutia Tree Leaf Extracts

The size, density, distribution, shape, formation, and orientation at different calcination temperatures for ZnO nanoparticles have been studied by using the FESEM analysis, as shown in Figure 4. It can be observed that the ZnO nanoparticles were formed by using Pinus Brutia tree leaf extraction and modified by increasing several calcination temperatures from 200 ºC to 500 ºC. Also, it is noticeable from Figures 4 (a) to 4 (c) that the ZnO NPs were successfully produced with high density and had a high rate of agglomeration due to the electrostatic charge. Due to a high agglomeration rate, the average size distribution was not estimated for the ZnO NPS samples synthesized with calcination temperatures 200, 300, an. The agglomeration makes the NPs stick together, making it challenging to observe the NPs. Whereas, the shape and size of Zinc oxide nanoparticles increase with increasing the calcination temperature. The novelty of this study is giving a good idea about understanding the calcination temperature of the final product of ZnO NPs.

In Figure 4, as the calcination temperature increases, one can clearly understand that the calcination temperature plays an essential role in the deagglomeration of the ZnO NPs.

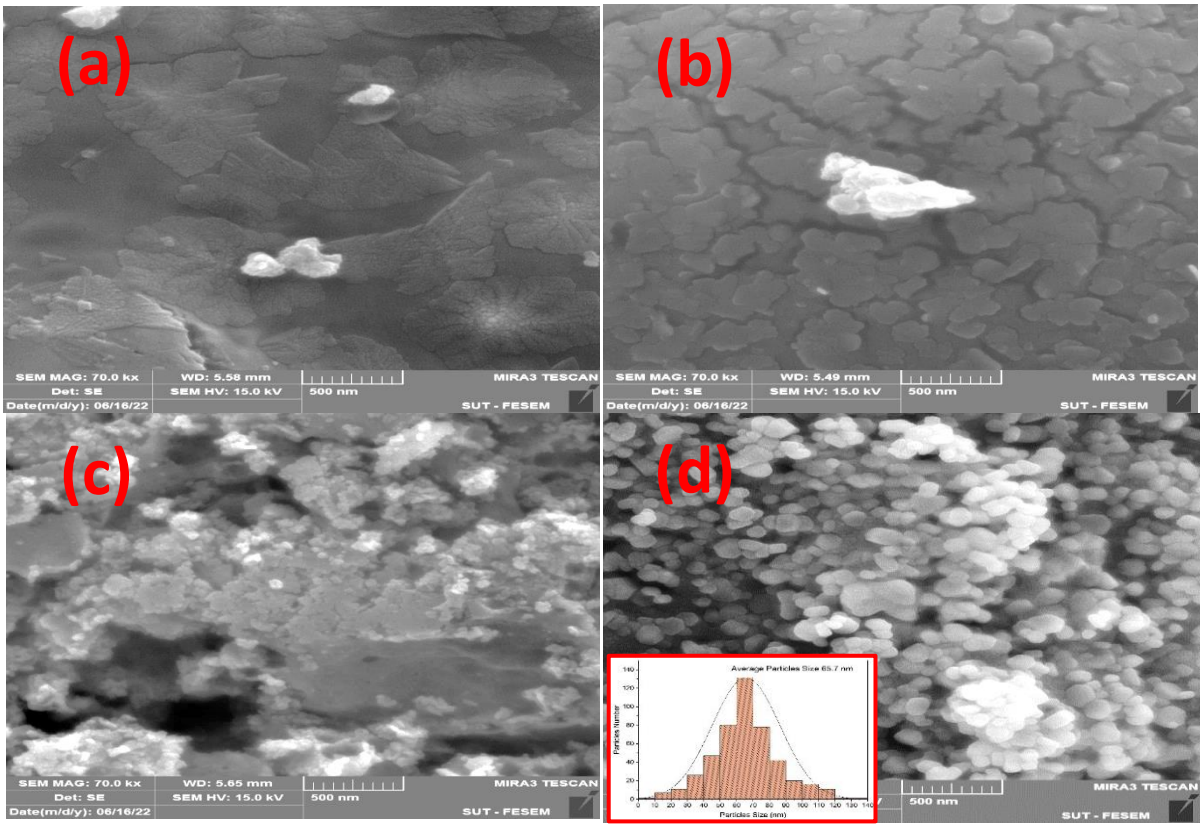

Figure 4. The effect of Various Calcination Temperatures on the Morphological Properties of Zinc Oxide Nanoparticles Produced by utilizing the leaf Extracts of the Tree of Pinus Brutia: (a) 200 ºC, (b) 300 ºC, (c) 400 ºC, and (d) 500 ºC.

The green synthesis nanoparticles, distinguished by significant aggregation formation, are where ZnO NPs are typically found. This is a result of the larger surface area and lasting affinities of biosynthetic NPs that cause them to clump or aggregate together (Vidya et. al. 2013). One might assert that ecological factors significantly affect stability and NP agglomeration. As a result, as the nanoparticles grew, they came together, and a symmetrical cluster appeared on its own (Shim et. al., 2019). While the calcination temperature the size, shape, and other characteristics have been studied. When the temperature is increased to 500 ºC, the ZnO NPs have been in spherical shapes, and the majority of these NPs were gathered together to form clusters with high distribution densities as shown in figure 4, which shows that the ZnO NPs have narrow size distribution, shape, and low rate of agglomerations. They have an average size of about 65.70 nm.

The elementally chemical composition of the biosynthesized ZnO NPs is investigated and evaluated using EDX spectroscopic analysis in different calcination temperatures in the range of (200-500) ºC. One can notice that the EDX analysis. It is apparent that both the Oxygen (O) and Zinc (Zn) elements are present, eliminating the possibility of any impurity's indicators with respect to the orientation of the features structures of the green synthesis ZnO NPs. The Au energy was observed because the ZnO NPs were coated with gold NPs before taking the EDX and FESEM analysis.

ZnO nanoparticles exhibit unique features, as evidenced by the two highly directed Zn peaks in the EDX spectrums that were about 1.1 and 8.7 keV and an oxygen signal at 0.5 keV (Amad et. al., 2022). All green synthesis ZnO NPs made at different pH levels have approximately the same zinc (Zn) to oxygen (O) atomic ratio. Quantitative characterizations from (EDX) show that the studied nanoparticles are pure GS ZnO because the computed (MR) molecular ratio of Zinc. Oxygen in the generated nanoparticles is 1:1. The weight percentage of GS ZnO nanoparticles composition has been obtained using EDX analysis at numerous calcination temperatures which are Zn (70.2%, 70.8%, 82.6%, and 82.4%) and O (29.8%, 29.2%, 17.4%, and 17.6%) for calcination temperatures 200 ºC, 300 ºC, 400 ºC, and 500 ºC, respectively.

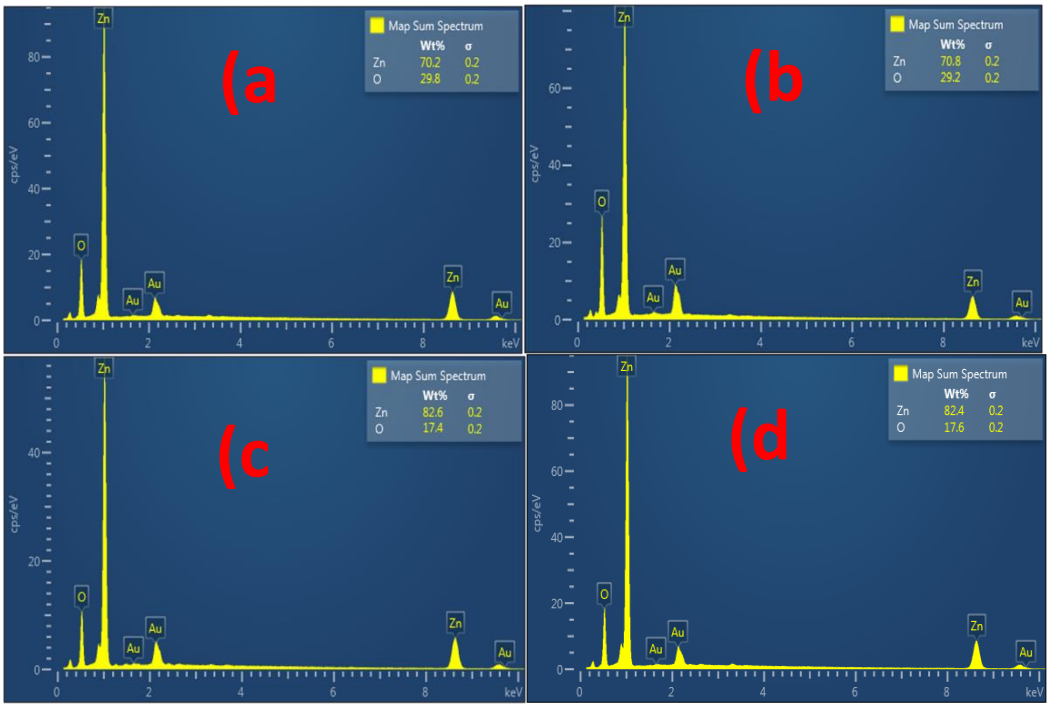

Figure 5. The effect of the Various Calcination Temperatures on the Elemental Chemical Compositions (EDS)of Zinc Oxide Nanoparticles Produced by utilizing the leaf Extracts of the of Pinus Brutia Tree: (a) 200 ºC, (b) 300 ºC, (c) 400 ºC, and (d) 500 ºC.

The structural properties of the fabricated ZnO NPs from Pinus Brutia plant leaf extracts with various calcination temperatures were investigated using the non-distractive XRD technique, as shown in Figure 6. The investigated diffractions for all XRD patterns of ZnO NPs were biosynthesized with hexagonal (wurtzite) polycrystalline crystal structures and indexed with the standard XRD database (JCPDS card number 98-009-4004).

Further evidence that the ZnO NPs made from Pinus Brutia tree leaf extracts at various calcination temperatures were formed with extremely high purity of ZnO nanocrystal phases came from the lack of peak diffraction from other defects (impurities). Figure 6 shows that (100), (002), and (101), which are the three main and firm diffraction peaks with changing intensities that are present in the X-ray diffraction peaks for all calcination temperatures, changed in intensity as the ZnO NPs were calcinated at various temperatures. The diffraction peaks along the (101) plane are also more apparent and robust; also, the XRD results and behaviors displayed are completely consistent with other studies (Barzinjy et. al., 2020, Dey et. al., 2022, Abdo et. al. 2021, Abel et. al. 2021).

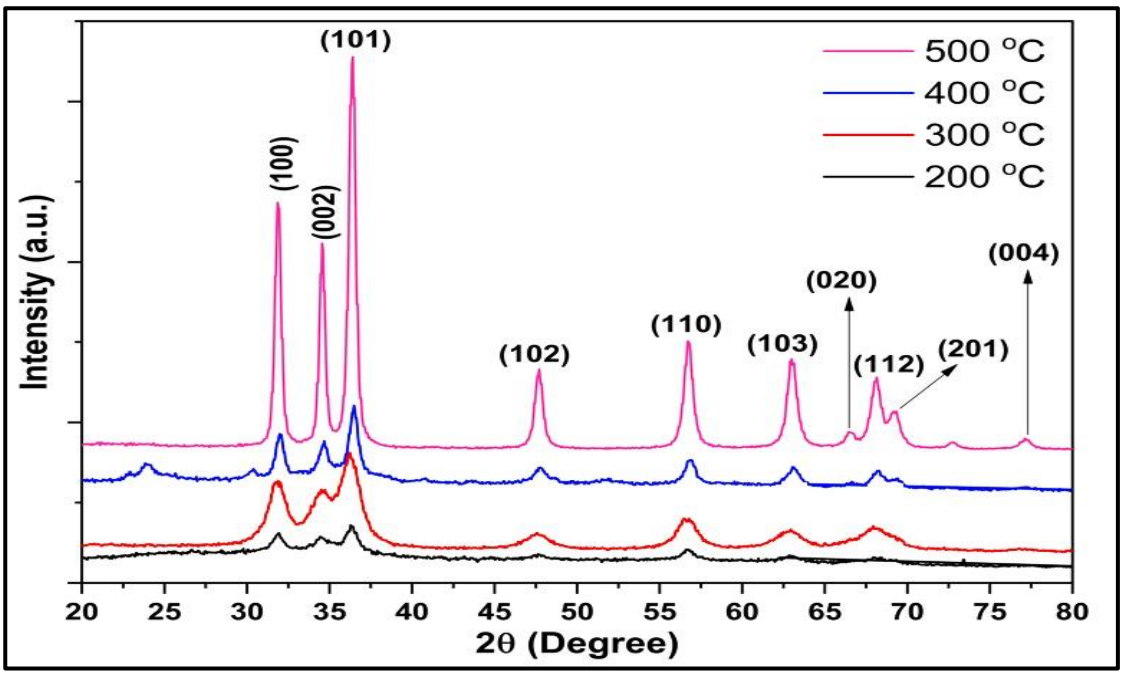

Figure 6. The effect of the Various Calcination Temperatures on the XRD Patterns of Zinc Oxide Nanoparticles Produced by utilizing the leaf Extracts of the Tree of Pinus Brutia

The average particle size of ZnO NPs produced at various calcination temperatures of the three dominant planes, (100), (002), and (101), is determined using the Debye-Scherrer equation (Abdulrahman et. al., 2020). Table 1 displays the results of (D).

$$D = \frac{k\lambda}{\beta\cos\theta} \quad (1)$$

where K, D, the angle of diffraction, the wavelength of the X-ray beam, and the shape factor of the crystallite are, in turn, the (FWHM) Full Width at Half Maximum of the peak, respectively.

When ZnO NPs are calcinated from 200 ºC to 500 ºC, the average particle size has been changed. The annealing process causes the particles to reorient due to heat energy, which also helps to reduce crystal structural flaws. At the same time, it results in variations in the average size of the particles of ZnO NPs (Korake et. al. 2014).

The dislocation density (δ) of ZnO NPs produced with various calcination temperatures in the range between (200 to 500) ºC, which is computed using the equation below, coupled with the dislocation density of synthesized ZnO NPs (Abdulrahman et. al., 2020), represents the number of defects present in the ZnO NPs nano-powder that is caused by internal strain. The obtained results of (δ) have been listed in Table 1:

$$\delta = \frac{1}{D^2} \quad (2)$$

Where D is the crystallite size

From Table 1, one can conclude that the calcination temperature significantly affects the number of defects present in the Zinc Oxide NPs. The following equations (Abdulrahman et. al., 2020) have been implemented to evaluate the effect of various calcination temperatures on the length of the bond as well for hexagonal-cell volume of produced ZnO nanoparticles along the planes of (100), (002), and (101). The results are reported in Table 1.

$$L = \sqrt{\frac{a^2}{3} + \left(\frac{1}{2} - u\right)^2 c^2} \quad (3)$$

The length of the "c" axis is a parameter related to the ratio of "c/a," and "u" represents the distance that the atoms traveled in the direction of the subsequent atoms, according to the formula below (Abdulrahman et. al., 2020);

$$u = \frac{a^2}{3c^2} + 0.25 \quad (4)$$

To investigate (V) the hexagonal cell's volume, the below formula has been employed (Abdulrahman et. al., 2020):

$$V = \frac{\sqrt{3}}{2} a^2 c \quad (5)$$

Table 1: The effects of the calcination temperatures on the ZnO nanoparticle's volume, bond length, dislocation density, crystal size, and (100), (002), and (003) peak diffraction planes (101)

Calcination Temperature (ºC)	Plane	D (nm)	δ ×10^{-5} (Å^{-2})	V(Å^3)	L (Å)
200	100	23.989	1.737	50.946	2.025
300	100	41.951	0.568	52.318	2.044
400	100	20.989	2.269	51.033	2.027
500	100	23.991	1.737	50.814	2.024
200	002	21.131	2.239	40.674	1.879
300	002	10.563	8.961	40.903	1.883
400	002	16.914	3.495	40.003	1.869
500	002	24.154	1.714	40.468	1.875
200	101	42.488	0.554	34.759	1.783
300	101	33.974	0.866	35.218	1.791
400	101	21.248	2.215	34.546	1.779
500	101	24.286	1.700	34.489	1.778

By applying Bragg's law (Ahmed et. al., 2020), (a & c) the lattice constants, with the three main planes (100), (002), and (101) of hexagonal Zinc Oxide NPs structure with various

calcination temperatures have been calculated. The results of (a & c) are shown in Table 2.

$$a = \sqrt{\frac{1}{3}}\frac{\lambda}{\sin\theta} \quad (6)$$

$$c = \frac{\lambda}{\sin\theta} \quad (7)$$

The diffraction peak's angle is denoted by the symbol " ɵ" and " λ " also denotes the X-ray source's wavelength.

Because of the following equations (Ahmed et. al., 2020), the strains (ƹc) and (ƹa), the main planes of the a-axis and c-axis, respectively, of the Zinc Oxide Nanoparticles produced at different calcination temperatures, are considered. The results of (ƹc) and (ƹa) are listed in Table 2.

$$\varepsilon_a = \frac{a-a_o}{a_o} \times 100\% \quad (8)$$

$$\varepsilon_c = \frac{c-c_o}{c_o} \times 100\% \quad (9)$$

a_o and c_o are indicated as the standard lattice constants targeted in the database. There are unbound Zinc Oxide Nanoparticles everywhere.

A compressive strain has been defined as a negative strain value, which includes lattice growth. While the expansion in the lattice is shown by the positive sign of the strain value, it is connected to the tensile strain (Ahmed et. al., 2020; Ahmed et. al., 2021). The inter-planer distance of biosynthesized ZnO NPs is significantly impacted by increasing the calcination temperature, as shown in Table 2, which provides further evidence. To study this, the following equation (Ahmed et. al., 2021) has been used:

$$\frac{1}{d^2} = \frac{4}{3}\left(\frac{h^2+hk+k^2}{a^2}\right) + \frac{l^2}{c^2} \quad (10)$$

Anywhere h, k, and l are situated Miller indices as per X-Ray diffraction peaks.

Table 2: Impact of Several Calcination Temperatures on the Lattice Parameters and Zinc Oxide (wurtzite-hexagonal) Structure properties of the produced Zinc Oxide Nanoparticles with the Sharper Peaks Diffraction planes of (100), (002), and (101)

Calcination Temperature (ºC)	Plane	FWHM	2θ	c (Å)	ƹc%	a (Å)	ƹa%	d (Å)
200	100	0.3444	31.883	5.609	7.807	3.238	-0.262	2.805
300	100	0.1968	31.5944	5.659	8.766	3.267	0.625	2.829
400	100	0.3936	31.8645	5.612	7.868	3.240	-0.206	2.806
500	100	0.3444	31.9114	5.604	7.714	3.236	-0.349	2.802
200	002	0.3936	34.4427	5.203	0.011	3.004	-7.474	2.602
300	002	0.7872	34.3765	5.213	0.198	3.009	-7.302	2.606
400	002	0.492	34.6403	5.175	-0.542	2.987	-7.986	2.587
500	002	0.3444	34.5031	5.195	-0.158	2.999	-7.631	2.597
200	101	0.1968	36.3581	4.938	-5.092	2.851	-12.197	2.469
300	101	0.246	36.194	4.959	-4.677	2.863	-11.812	2.479
400	101	0.3936	36.4351	4.928	-5.286	2.845	-12.376	2.463
500	101	0.3444	36.4558	4.925	-5.339	2.844	-12.424	2.463

The optical characteristics of GS ZnO NPs which were calcinated with different temperatures from 200 ºC to 500 ºC were studied using the double beam UV-Visible spectrophotometer by observing the absorption spectrum. The absorption spectrums of GS ZnO NPs produced using extracts of the leaf of PB tree at different calcination temperatures in the wavelength range between (300 to 800) nm is shown in Figure 7. The GS ZnO NPs powder exhibits strong (UV) absorption, a high rate of absorbance less than 400 nm, remarkable clarity, and a narrow visible absorption range when the calcination temperature is varied (Roza et. al., 2015).

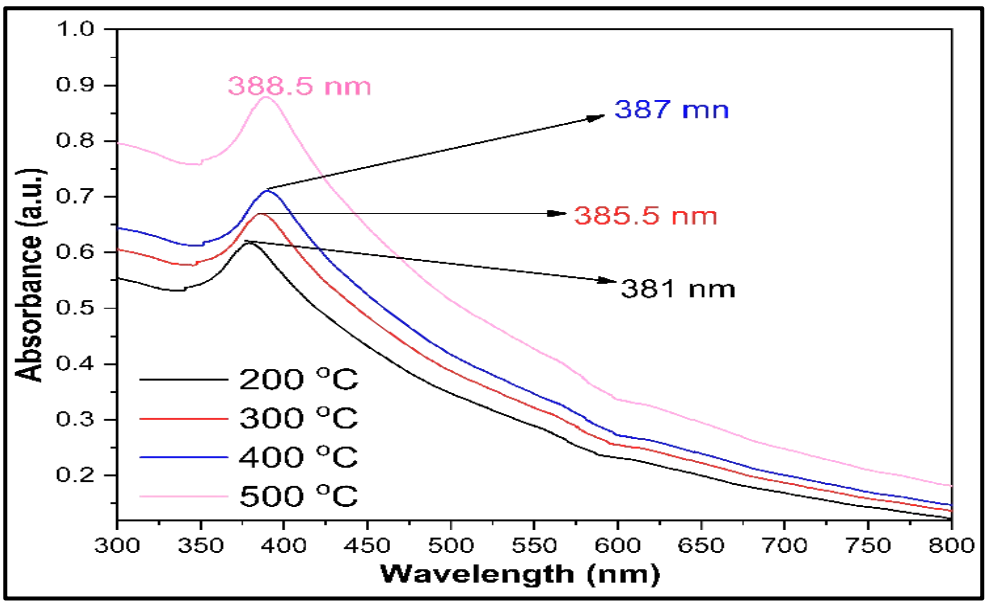

Figure 7. The effect of the Various Calcination Temperatures on the Optical Absorption Properties of Zinc Oxide Nanoparticles Produced by utilizing the leaf Extracts of the Tree of Pinus Brutia

Low absorption values at long wavelengths are caused by defects in GS ZnO NP that rely on the crystal's quality, lattice parameters, crystal size, and oxygen vacancies that exist as donor impurities (Shabannia et. al., 2014). In the wavelength range of (381-388.5) nm, exciton absorption and a strong UV absorption edge have been observed. These phenomena are connected to the (Eg) optical Energy Band-gap of the GS ZnO nanoparticles at varied calcination temperatures. When the peak is sharpened, monodispersed ZnO NPs are produced as a result of the (SPR). Rather than following the rule of thumb, the maximum peak absorption of Zinc Oxide Nanoparticles was discovered to be in the range between 350 and 400 nm. The value obtained is smaller than the one that bulk Zinc Oxide anticipated using 381 nm to 388.5 nm wavelengths, and it also exhibited a blue shift in excitonic absorption, suggesting a slight quantum confinement effect (Barzinjy et. al., 2020).

Figure 8 illustrates the projection of the linear component of $(\alpha h\nu)^2$ versus (h) using transmittance spectra. The Tauc formula is then used to determine the optical band-gap energy of GS ZnO NPs using PB tree leaf extracts at various calcination temperatures (Abdulrahman et. al., 2022):

$$(\alpha h\nu)^2 = A(h\nu - E_g)^n \quad (11)$$

Where α, hv, A and E_g are the absorption coefficient, photon's energy, constant, and optical band gap energy. Also, n depends on the transmission, and it is equal to 1/2 for allowed direct transmission.

The (α) coefficient container's major focus is the transmittance spectrum, which is used in conjunction with (Abdulrahman et. al., 2022).

$$\alpha = \frac{\ln(\frac{1}{T})}{d} \quad (12)$$

"T "and "d" are the transmittances and thickness aimed at ZnO samples,

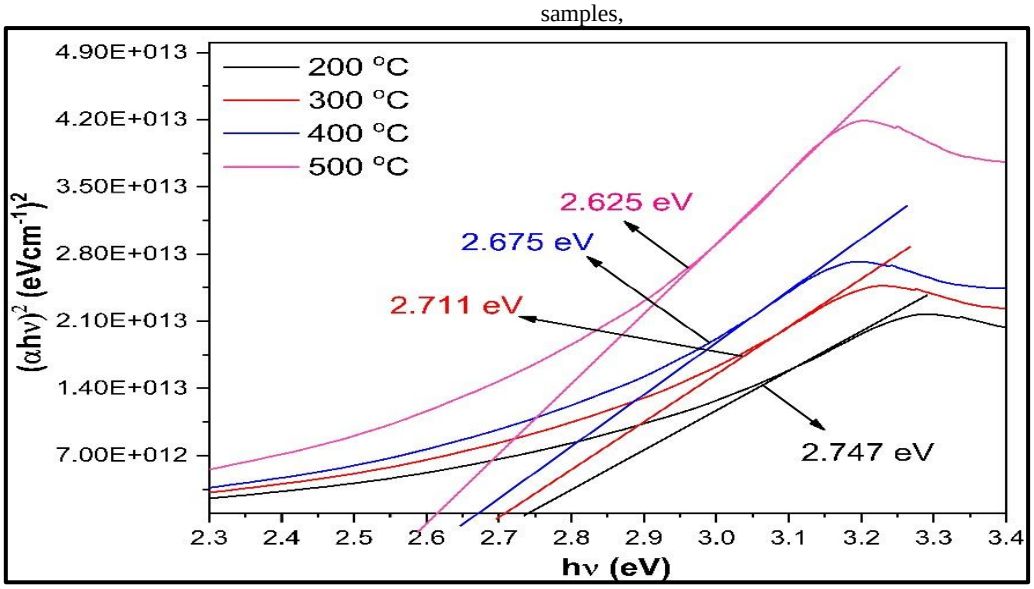

Figure 8. The Influence of the Different Calcination Temperatures on the Optical Energy Band Gap of Zinc Oxide Nanoparticles Produced by utilizing the leaf Extracts of the Tree of Pinus Brutia. Tauc-plot Versus Eg.

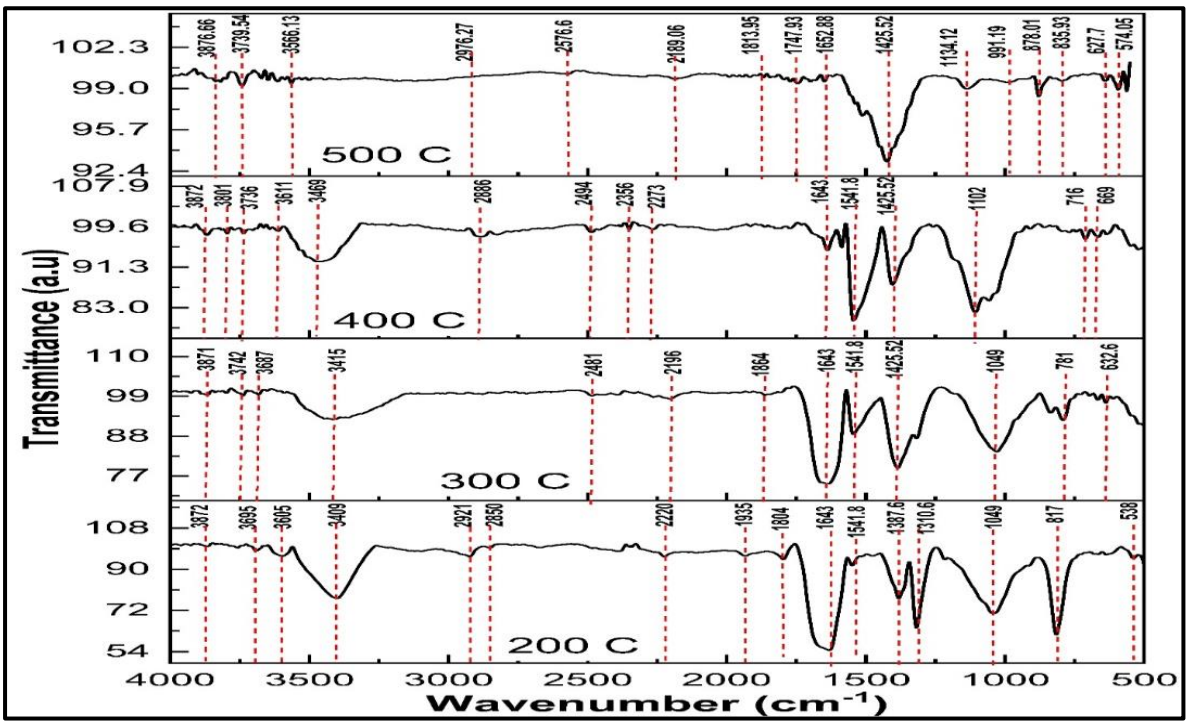

Figure 9. FTIR Spectrum Analysis of the Zinc Oxide Nanoparticles synthesized using the extracts of the leaf of the Pinus Brutia Tree when Calcinated with several Temperatures

From Figure 8, one can see that the transition region of the produced GS ZnO NPs with various calcination temperatures is roughly in the range of (2.65-2.7) eV, which is represented by the Eg corresponding to the transition band between both valance and conduction bands, that denotes the Eg of the semiconductor ZnO NPs (Roza et. al., 2015). Also, from the plots in Figure 8, the obtained Eg of synthesized GS ZnO NPs with different calcination temperatures are (2.747, 2.711, 2.675, and 2.625) eV, and (200, 300, 400, and 500) ^{o}C, respectively. The Eg is decreased with increasing the calcination temperature from 200 ^{o}C to 500 ^{o}C. This decrease in the Eg of the nanoparticles is due to the change in the lattice constant of the tree's leaf extracts; because of the use of plant extracts, a lowering in the band gap is expected (Khan et. al., 2019). This discovery, which was made primarily in GS NPs, is not contradictory with quantum (effect) confinement occurrences. GS NPs are typically more active than NPs produced by other fabrication methods.

FTIR spectrum analysis has been employed to examine and study the functional group, purity, and composition of the obtained ZnO nanoparticles produced via the GS technique, and by displaying in Figure 9. Figure 9 demonstrates that no peaks were apparent in the observation range and showed the purity of the GS ZnO nanoparticles which were calcinated with different temperatures. The FTIR spectrum of ZnO NPs calcinated with the temperature of 200 ^{o}C shows different absorption peaks. The peaks 538 cm^{-1} and 817 cm^{-1} are related to the Aliphatic Iodo compounds, C-I stretch, peroxides, and C-O-O- stretch, respectively. Also, the obtained peaks (1049, 1310, 1387,1541, 1643, 1804, and 1935) cm^{-1} are related to compounds of Primary amine, CN stretch, Aromatic tertiary amine, CN stretch, Common inorganic ions, Nitrate ion, Carboxylate (carboxylic acid salt), Quinone or conjugated ketone of Carbonyl compound, cm^{-1} Carbonyl compound of Acid (acyl) halide, and Aromatic ring (aryl) of Aromatic combination bands, respectively. The investigated peak (2220, 2850, 2921, 3409, 3605, 3695, and 3872) cm^{-1} are related to the compound of C≡C Medial alkyne (disubstituted), Methoxy, C-H stretch (CH3-O-), Methylene C-H asym./sym, Stretch, Normal ''polymeric'' OH stretch, Nonbonded hydroxy group, OH stretch, Primary alcohol, OH stretch, and O-H stretching of alcohol, respectively.

The FTIR spectrum of ZnO NPs shows several absorption peaks, which include (632, 781, 1049, 1425, 1541, 1643, and1864) cm^{-1} that are related to Acetylenic(alkyne) of Alkyne C-H bend, Aromatic ring (aryl) of C-H 1,3-Disubstitution (meta), Primary amine, CN stretch, Methylene (>CH2) of Methylene C-H bend, Carboxylate (carboxylic acid salt), Quinone or conjugated ketone of Carbonyl compound, and Carbonyl compound of Acid (acyl) halide, respectively. While the obtained peaks (2196, 2481, 3415, 3687, 3742, and 3871) cm^{-1} were related to the compounds C≡C Medial alkyne (disubstituted), strong O=C=O stretching carbon dioxide, Normal ''polymeric'' OH stretch, Nonbonded hydroxy group, OH stretch, Primary alcohol, OH stretch, and O-H stretching of alcohol, respectively.

Different absorption peaks were seen in the ZnO Nanoparticles' FTIR spectrum that was calcinated with the temperature of 400 ^{o}C as shown in Figure 9. The observed peaks were (669, 716, 1102, 1425, 1541, and 1643) cm^{-1} that were related to the compounds of Acetylenic(alkyne) of Alkyne C-H bend, Aromatic ring (aryl) of C-H 1,3-Disubstitution (meta), Secondary alcohol, C-O stretch, Common inorganic ions of Carbonate ion, Nitrogen-oxy compounds of Aliphatic nitro compounds, and Quinone or conjugated ketone of Carbonyl compound, respectively. While peaks (2273, 2356, 2494, 2886, 3469, 3611, 3736, 3801, and 3872) cm^{-1} are concerned with C≡C Medial alkyne (disubstituted), stretching O=C=O carbon dioxide, strong O=C=O stretching carbon dioxide, Methoxy, C-H stretch (CH3-O-), Normal ''polymeric'' OH stretch, Nonbonded hydroxy group, OH stretch, Primary alcohol, OH stretch, and O-H stretching of alcohol, respectively.

In addition, when ZnO NPs are calcinated at 500 oC, several absorption peaks are investigated, as shown in Figure 9. The absorption peaks observed at (574, 627, 835, 878, and 991) cm-1 are related to the Disulfides (C-S stretch), and Alkyne C-H bend, Peroxides, C-O-O- stretch band, and Aromatic C-H in-plane bend, respectively. Additionally, the seven peaks absorption were seen in the (1000-2000) cm-1, which are (1134, 1343, 1425, 1521, 1652, 1747, and 1813) cm-1 that are owing to the bands of

the Aliphatic fluoro compounds, C-F stretch primary or secondary, OH in-plane band, Carbonate ion of Common inorganic ions, Carboxylate (carboxylic acid salt), Amide of Carbonyl compound, Ester of Carbonyl compound, and Acid (acyl) halide, respectively. Additionally, the examined absorption peak lies in the region between 2000 cm-1 to 4000 cm-1, including (2189, 2870, 2976, 3566, 3739, and 3876) cm-1, which are related to the bands of Cyanide ion, thiocyanate ion, related ions, Methyl C-H asym./sym, Stretch, internally bonded OH stretch, and O-H stretching of alcohol, respectively.

4. CONCLUSION

The ZnO NPs have been successfully produced at a low cost using the extracts from the leaf of the Pinus Brutia tree. The influence of the tree extracts from PB and ZnO NPs' properties, including their crystal structure, size, orientation, average size, shape, density distribution, functional group, elemental composition, and optical characteristics, have been studied at various calcination temperatures. According to the PB tree leaf extracts analysis, the PB tree is a better option for the biosynthesis of GS Zinc Oxide Nanoparticles at different calcination temperatures. Also, the results displayed that the change in the calcination (annealing) temperature significantly affects all of the obtained properties of the ZnO NPs. The calcination temperature change greatly impacts the quality and average crystal size of the generated hexagonal-wurtzite Zinc Oxide Nanoparticles. The FESEM analysis showed that the Zinc Oxide Nanoparticles are significantly affected in their orientation, shape, and size by the calcination temperatures. The GS ZnO nanoparticles' UV-Visible analysis revealed a significant peak for all Zinc Oxide NPs made at various temperatures of calcination, a considerable absorbance in the UV region and below 400 nm, and a poor absorption rate in the visible region. The (Eg), which denotes the Energy Band Gap, lays between the (2.65-2.747) eV region, and it decreases as the calcination temperature increases.

Additionally, the FTIR spectra of formed ZnO NPs with various calcination temperatures showed no apparent peak in the visible range, demonstrating pure Zinc Oxide Nanoparticles produced by employing PB tree leaf extracts. In addition, according to all of the investigated results and properties of the Zinc Oxide Nanoparticles, the Zinc Oxide Nanoparticles that are calcinated at 500 oC had higher quality. They performed better than those made at other calcination temperatures.

REFERENCES

[1] Azeez Abdullah Barzinjy, Samir Mustafa Hamad, Ahmed Fattah Abdulrahman, Safiya Jameel Biro, and AbdulBasit Ali Ghafor, "Biosynthesis, Characterization and Mechanism of Formation of ZnO Nanoparticles Using Petroselinum Crispum Leaf Extract", Current Organic Synthesis, 2020, 17, 558-566. https://doi.org/10.2174/1570179417666200628140547.

[2] Abdelbaky, A.S.; Abd El-Mageed, T.A.; Babalghith, A.O.; Selim, S.; Mohamed, A.M.H.A. Green Synthesis and Characterization of ZnO Nanoparticles Using Pelargonium odoratissimum (L.) Aqueous Leaf Extract and Their Antioxidant, Antibacterial and Anti-inflammatory Activities. Antioxidants 2022, 11, 1444.

[3] Khan, I.; Saeed, K.; Khan, I. Nanoparticles: Properties applications and toxicities. Arab. J. Chem. 2019, 12, 908–931.

[4] Nilavukkarasi, M.; Vijayakumar, S.; Prathipkumar, S. Capparis zeylanica mediated bio-synthesized ZnO nanoparticles as antimicrobial photocatalytic and anti-cancer applications. Mater. Sci. Technol. 2020, 3, 335–343.

[5] Zheng, X.; Yuhui, W.; Ling, S.; Arunachalam, C.; Sulaiman, A.; Liwei, F. Anticarcinogenic effect of zinc oxide nanoparticles synthesized from Rhizoma paridis saponins on Molt-4 leukemia cells. J. King Saud Univ. Sci. 2020, 32, 1865–1871.

[6] A. Waseem and K. Divya, "Green synthesis, characterization and anti-microbial activities of ZnO nanoparticles using Euphorbia hirta leaf extract," Journal of King Saud University Science, vol. 32, no. 4, pp. 2358–2364, 2020.

[7] S. Bettini, R. Pagano, V. Bonfrate, E. Maglie, D. Manno, A. Serra, L. Valli, G. Giancane, promising piezoelectric properties of new ZnO@ octadecylamine adduct, The Journal of Physical Chemistry C 119(34) (2015) 20143-20149.

[8] H. Hong, J. Shi, Y. Yang, Y. Zhang, J.W. Engle, R.J. Nickles, X. Wang, W. Cai, Cancer-targeted optical imaging with fluorescent zinc oxide nanowires, Nano letters 11(9) (2011) 3744-3750.

[9] Meron Girma Demissie, Fedlu Kedir Sabir, Gemechu Deressa Edossa, and Bedasa Abdisa Gonfa, Synthesis of Zinc Oxide Nanoparticles Using Leaf Extract of Lippia adoensis (Koseret) and Evaluation of Its Antibacterial Activity, Journal of Chemistry,
Vol. 2020, Article ID 7459042, 9 pages. https://doi.org/10.1155/2020/7459042

[10] M. Seyyed, H. M. Tabrizi, E. Behrouz, and J. Vahid, "Biosynthesis of pure zinc oxide nanoparticles using Quince seed mucilage for photocatalytic dye degradation," Journal of Alloys and Compounds, vol. 821, Article ID 153519, 2020.

[11] Karam, S.T.; Abdulrahman, A.F. Green Synthesis and Characterization of ZnO Nanoparticles by Using Thyme Plant Leaf Extract. Photonics 2022, 9, 594. https://doi.org/10.3390/photonics9080594.

[12] Amad Nori Abdulqudos, Ahmed Fattah Abdulrahman, Biosynthesis and Characterization of ZnO Nanoparticles by using Leaf Extraction of Allium Calocephalum Wendelbow Plant, Passer 4 (Issue 2) (2022) 113-126. https://doi.org/10.24271/psr.2022.343112.1136.

[13] A. J. Aswathy, T. R. Achuthsankar. S. Nair. "Green synthesis and characterization of zinc oxide nanoparticles using Cayratia pedata leaf extract", Biochemistry and Biophysics Reports,v ol. 26, pp. 100995, 2021.

[14] A.A. Barzinjy, H. H. Azeez. "Green synthesis and characterization of zinc oxide nanoparticles using Eucalyptus globulus Labill. leaf extract and zinc nitrate hexahydrate salt", SN Applied Sciences, vol. 2, no.99, 2020. https://doi.org/10.1007/s42452-020-2813-1.

[15] R. Norouzi, M. Hejazy, and A. Ataei. "Scolicidal effect of zinc oxide nanoparticles against hydatid cyst protoscolices in vitro," Nanomedicine Research Journal, vol. 4, no.1, pp. 23–28, 2019. https://doi:10.22034/NMRJ.2019.01.004.

[16] V. Srivastava, D. Gusain, and Y. C. Sharma. "Synthesi s, characterization and application of zinc oxide nanoparticles (n-ZnO)," Ceramics International, vol. 39, no. 8, pp. 9803–9808, 2013. https://doi:10.1016/j.ceramint.2013.04.110.

[17] S. Zandi, P. Kameli, H. Salamati, H. Ahmadvand, and M. Hakimi. "Microstructure and optical properties of ZnO nanoparticles prepared by a simple method," Physica B: Condensed Matter, vol. 406, no.17, pp. 3215–3218, 2011. https://doi: 10.1016/j.physb.2011.05.026.

[18] J. P. Kim, I. K. Lee, B. S. Yun, S. H. Chung, G. S. Shim, H. Koshino, I. D. Yoo. "Ellagic acid rhamnosides from the stem bark of Eucalyptus globulus", Phytochemistry, vol. 57, pp.587–591, 2001.

[19] P. Singh, Y. J. Kim, D. Zhang, D. C. Yang. "Biological synthesis of nanoparticles from plants and microorganisms", Trends Biotechnol, vol. 34, pp.588–599. 2016.

[20] R. Hocine, J. Mazauric, K. Madani, L. Boulekbache-Makhlouf. "Phytochemical analysis and antioxidant activity of Eucalyptus globulus: a comparative study between fruits and leaves extracts", J. Chem. Eng Bio Chemistry, vol. 1, pp.23–29, 2016.

[21] Pai, S. Photocatalytic zinc oxide nanoparticles synthesis using Peltophorum pterocarpum leaf extract and their characterization. Optik (Stuttg.), 2019, 185, 248-255. http://dx.doi.org/10.1016/j.ijleo.2019.03.101

[22] Vidya, C.; Hiremath, S.; Chandraprabha, M.N.; Antonyraj, M.L.; Gopal, I.V.; Jain, A.; Bansal, K. Green synthesis of ZnO nanoparticles by Calotropis gigantea. Int. J. Curr. Eng. Technol. 2013, 1, 118–120.

[23] Shim, Y.J. Zinc oxide nanoparticles synthesized by Suaeda japonica Makino and their photocatalytic degradation of methylene blue. Optik 2019, 182, 1015–1020.

[24] A. Dey and S. Somaiah, "Green synthesis and characterization of zinc oxide nanoparticles using leaf extract of Thryallis glauca (Cav.) Kuntze and their role as antioxidant and antibacterial", Microscopy Research and Technique, April 2022, https://doi.org/10.1002/jemt.24132.

[25] A. M. Abdo, A. Fouda, A. M. Eid, N. M. Fahmy, A. M. Elsayed, A. M. Khalil, O. M. Alzahrani, A. F. Ahmed, A.M. Soliman. "Green Synthesis of Zinc Oxide Nanoparticles (ZnO-NPs) by Pseudomonas aeruginosa and Their Activity against Pathogenic Microbes and Common House Mosquito, Culex pipiens", Materials (Basel), vol. 14, no. 22, pp. 6983, 2021. https://doi:10.3390/ma14226983.

[26] S. Abel, J. L. Tesfaye, R. Shanmugam, L. P. Dwarampudi, G. Lamessa, N. Nagaprasad, M.Benti, R. Krishnaraj. "Green Synthesis and Characterizations of Zinc Oxide (ZnO) Nanoparticles Using Aqueous Leaf Extracts of Coffee (Coffea arabica) and Its Application in Environmental Toxicity Reduction", J. of Nanomaterials, vol. 2021, ID 3413350, 6 pages, 2021. https://doi.org/10.1155/2021/3413350.

[27] A. F. Abdulrahman. "The Influence of Various Reactants in the Growth Solution on the Morphological and Structural Properties of ZnO Nanorods", Passer Journal, Vol. 2 (2), pp. 69-75, 2020. doi: 10.24271/psr.14.

[28] Korake, P.; Dhabbe, R.; Kadam, A.; Gaikwad, Y.; Garadkar, K. Highly active lanthanum doped ZnO nanorods for photodegradation of metasystox. J. Photochem. Photobiol. B Biol. 2014, 130, 11–19.

[29] A. F. Abdulrahman, S. M. Ahmed, A. A. Barzinjy, S. M. Hamad, N. M. Ahmed, M. A. Almessiere. "Fabrication and Characterization of High-Quality UV Photodetectors Based ZnO Nanorods Using Traditional and Modified Chemical Bath Deposition Methods", Nanomaterials, vol. 11, no.3, pp. 677, 2021. https://doi.org/10.3390/nano11030677.

[30] Ahmed F. Abdulrahman "The effect of different substrate-inclined angles on the characteristic properties of ZnO nanorods for UV photodetectors applications", Journal of Materials Science: Materials in Electronics, Vol.31 (17), 14357-14374, 2020.

[31] Ahmed Fattah Abdulrahman, Sabah Mohammed Ahmed, Samir Mustafa Hamad, Azeez Abdullah Barzinjy "Effect of Growth Temperature on Morphological, Structural, and Optical Properties of ZnO Nanorods Using Modified Chemical Bath Deposition Method", Journal of Electronic Materials, 50, 1482–1495 (2021).

[32] L. Roza, Y. A. Rahman, A. A. Umar, M. M. Salleh. "Direct growth of oriented ZnO nanotubes by self-selective etching at lower temperature for photo-electrochemical (PEC) solar cell application", J. of Alloys and Comps., vol. 618, pp.153, 2015.

[33] R. Shabannia, H.A. Hassan. "Characteristics of photoconductive UV photodetector based on ZnO nanorods grown on polyethylene naphthalate substrate by a chemical bath deposition method", Electron. Mater. Lett., vol. 10, pp.837–843, 2014. https://doi.org/10.1007/s13391-014-3245-0.

[34] A. F. Abdulrahman, N. M. Abd-Alghafour."Synthesis and characterization of ZnO nanoflowers by using simple spray pyrolysis technique", Solid-State Electronics, vol. 189, pp.108225, 2022. https://doi.org/10.1016/j.sse.2021.108225.

[35] M. M. Khan. "Potentials of Costus woodsonii leaf extract in producing narrow band gap ZnO nanoparticles", Material Science Semicondutor Process., vol. 91, pp. 194200, 2019.

[35] Kamal K. Taha; M. Al Zoman; M. Al Outeibi; S. Alhussain; A. Modwi; Abdulaziz A. Bagabas; "Green and Sonogreen Synthesis of Zinc Oxide Nanoparticles for The Photocatalytic Degradation of Methylene Blue in Water", NANOTECHNOLOGY FOR ENVIRONMENTAL ENGINEERING, 2019. (IF: 3)

[36] Happy Agarwal; Amatullah Nakara; Soumya Menon; VenkatKumar Shanmugam; "Eco-friendly Synthesis of Zinc Oxide Nanoparticles Using Cinnamomum Tamala Leaf Extract and Its Promising Effect Towards The Antibacterial Activity", JOURNAL OF DRUG DELIVERY SCIENCE AND TECHNOLOGY, 2019. (IF: 3)

[37] Aravapalli Vanaja; M. Suresh; Jaison Jeevanandam; Venkatesh; Sk. Gousia; D. Pavan; D. Balaji; N. Bhanu Murthy; "Copper-Doped Zinc Oxide Nanoparticles for The Fabrication of White LEDs", PROTECTION OF METALS AND PHYSICAL CHEMISTRY OF SURFACES, 2019.

[38] K Kanimozhi; S Khaleel Basha; K Kaviyarasu; V SuganthaKumari; "Salt Leaching Synthesis, Characterization and In Vitro Cytocompatibility of Chitosan/Poly(vinyl Alcohol)/Methylcellulose - ZnO Nanocomposites Scaffolds Using L929 Fibroblast Cells", JOURNAL OF NANOSCIENCE AND NANOTECHNOLOGY, 2019. (IF: 3)

[39] Geeta Gahlawat; Anirban Roy Choudhury; "A Review on The Biosynthesis of Metal and Metal Salt Nanoparticles By Microbes", RSC ADVANCES, 2019. (IF: 5)

[40] Wencai Zhou; Xueying Qiu; Yuheng Jiang; Yingying Fan; Shilei Wei; Dongxue Han; Li Niu; Zhiyong Tang; "Highly Selective Aerobic Oxidation of Methane to Methanol Over Gold Decorated Zinc Oxide Via Photocatalysis", JOURNAL OF MATERIALS CHEMISTRY, 2020. (IF: 3)

[41] Shriniwas P. Patil; Subhash T. Kumbhar; "Vitex Negundo Assisted Green Synthesis of Metallic Nanoparticles with Different Applications: A Mini Review", FUTURE JOURNAL OF PHARMACEUTICAL SCIENCES, 2020.

[42] Amit Kumar Chauhan; Navish Kataria; V K Garg; "Green Fabrication Of ZnO Nanoparticles Using Eucalyptus Spp. Leaves Extract And Their Application In Wastewater Remediation", CHEMOSPHERE, 2020. (IF: 3)

[43] Anithadevi Sekar; Rakhi Yadav; "Green Fabrication of Zinc Oxide Supported Carbon Dots for Visible Light-Responsive Photocatalytic

Decolourization of Malachite Green Dye: Optimization and Kinetic Studies", OPTIK, 2021.
[44] Ashmalina Rahman; Mohammad Hilni Harunsani; Ai Ling Tan; Mohammad Mansoob Khan; "Zinc Oxide and Zinc Oxide-based Nanostructures: Biogenic and Phytogenic Synthesis, Properties and Applications", BIOPROCESS AND BIOSYSTEMS ENGINEERING, 2021.
[45] Gezahegn Faye; Tola Jebessa; Tilahun Wubalem; "Biosynthesis, Characterisation and Antimicrobial Activity of Zinc Oxide and Nickel Doped Zinc Oxide Nanoparticles Using Euphorbia Abyssinica Bark Extract", IET NANOBIOTECHNOLOGY, 2021.
[46] Hadiza Abdullahi Ari; Alani Olushola Adewole; Adamu Yunusa Ugya; Otaru Habiba Asipita; Makiyyu Abdullahi Musa; Wei Feng; "Biogenic Fabrication and Enhanced Photocatalytic Degradation of Tetracycline By Bio Structured ZnO Nanoparticles", ENVIRONMENTAL TECHNOLOGY, 2021.
[47] Amany M Diab; Basma T Shokr; Mustafa Shukry; Foad A Farrag; Radi A Mohamed; "Effects of Dietary Supplementation with Green-Synthesized Zinc Oxide Nanoparticles for Candidiasis Control in Oreochromis Niloticus", BIOLOGICAL TRACE ELEMENT RESEARCH, 2022.
[48] Ibrahem M A Hasan; Ahmed R Tawfik; Fawzy H Assaf; "GC/MS Screening of Buckthorn Phytochemicals and Their Use to Synthesize ZnO Nanoparticles for Photocatalytic Degradation of Malachite Green Dye in Water", WATER SCIENCE AND TECHNOLOGY : A JOURNAL OF THE INTERNATIONAL ASSOCIATION ON WATER POLLUTION RESEARCH, 2022.
[49] Muhammad Irfan; Hira Munir; Hammad Ismail; "Characterization and Fabrication of Zinc Oxide Nanoparticles By Gum Acacia Modesta Through Green Chemistry and Impregnation on Surgical Sutures to Boost Up The Wound Healing Process", INTERNATIONAL JOURNAL OF BIOLOGICAL MACROMOLECULES, 2022.
[50] Senthilkumar Chandrasekaran; Venkattappan Anbazhagan; Shanmugam Anusuya; "Green Route Synthesis of ZnO Nanoparticles Using Senna Auriculata Aqueous Flower Extract As Reducing Agent and Evaluation of Its Antimicrobial, Antidiabetic and Cytotoxic Activity", APPLIED BIOCHEMISTRY AND BIOTECHNOLOGY, 2022.
[51] Rahul Nitnavare; Joorie Bhattacharya; Sirikanjana Thongmee; Sougata Ghosh; "Photosynthetic Microbes in Nanobiotechnology: Applications and Perspectives", THE SCIENCE OF THE TOTAL ENVIRONMENT, 2022.
[52] Selvakumar Sakthivel; Anand Raj Dhanapal; Lilly Pushpa Paulraj; Annadurai Gurusamy; Baskar Venkidasamy; Muthu Thiruvengadam; Rajakumar Govindasamy; Mohammad Ali Shariati; Abdelhakim Bouyahya; Gokhan Zengin; Mohammad Mehedi Hasan; Pavel Burkov; "Antibacterial Activity of Seed Aqueous Extract of Citrus Limon (L.) Mediated Synthesis ZnO NPs: An Impact on Zebrafish (Danio Rerio) Caudal Fin Development", HELIYON, 2022.
[53] Dorcas Mutukwa; Raymond Taziwa; Lindiwe Eudora Khotseng; "A Review of The Green Synthesis of ZnO Nanoparticles Utilising Southern African Indigenous Medicinal Plants", Nanomaterials (Basel, Switzerland), 2022.
[54] Shahid Shabbir Awan; Rizwan Taj Khan; Ansar Mehmood; Muhammad Hafeez; Syed Rizwan Abass; Munazza Nazir; Muhammad Raffi; "Ailanthus Altissima Leaf Extract Mediated Green Production of Zinc Oxide (ZnO) Nanoparticles for Antibacterial and Antioxidant Activity", Saudi Journal Of Biological Sciences, 2022.